TECHNICAL RESEARCH REPORT

SYSTEMS RESEARCH CENTER

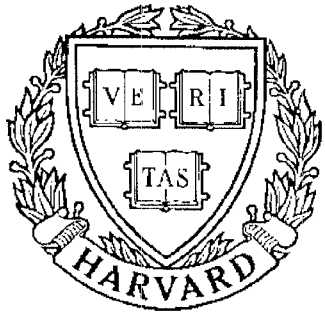

Supported by the National Science Foundation Engineering Research Center Program (NSFD CD 8803012), Industry and the University

Jacobian and Stiffness Analysis of a Novel Class of Six-DOF Parallel Minimanipulators

by F. Tahmasebi and L-W. Tsai

TR 92-84

JACOBIAN AND STIFFNESS ANALYSIS OF A NOVEL CLASS OF SIX-DOF PARALLEL MINIMANIPULATORS

Farhad Tahmasebi
Robotics Branch
NASA
Goddard Space Flight Center
Greenbelt, MD 20771
Associate Member of ASME

Lung-Wen Tsai
Mechanical Engineering Dept.
and Systems Research Center
University of Maryland
College Park, MD 20742
Fellow ASME

ABSTRACT

The Jacobian and stiffness matrices of two types of novel, six-DOF parallel minimanipulators are derived. A minimanipulator consists of three inextensible limbs, each of which is driven by a two-DOF driver. Bilinear stepper motors are used as drivers in the first type minimanipulator, whereas five-bar linkages are used as drivers in the second type minimanipulator. All of the minimanipulator actuators are base-mounted. Inextensible limbs (and five-bar linkage drivers in the second type minimanipulator) improve positional resolution and stiffness of the minimanipulators in certain directions. It is shown that, at the central configuration, the stiffness matrix of the first type minimanipulator can be diagonalized (decoupled). It is also shown that the first type minimanipulator can be designed to possess direct or torsional isotropic stiffness properties. Moreover, guidelines for designing the drivers of the second type minimanipulator are established.

1 INTRODUCTION

Parallel mechanisms have been used for applications in which the requirements for accuracy, rigidity, and load-to-weight ratio are more important than the need for a large workspace.

Stewart (1965) introduced his famous six-degree-of-freedom (six-DOF) platform as a motion simulator. Recently, many researchers have suggested the Stewart platform as a robot manipulator (e.g., Hunt, 1983; Fichter, 1986). Other six-DOF parallel manipulators have also been introduced and studied in the literature (e.g., Kohli et al., 1988; Hudgens and Tesar, 1988; Tsai and Tahmasebi, 1991a).

Dualities of serial and parallel manipulators were demonstrated by Waldron and Hunt (1987). For example, inverse kinematics of a serial manipulator is much more difficult than its direct kinematics; whereas, for a parallel manipulator, the opposite is true. Closed-form solutions have been obtained for direct kinematics of certain parallel manipulators (e.g., Griffis and Duffy, 1989; Nanua et al., 1990; Innocenti and Parenti-Castelli, 1990; Tahmasebi and Tsai, 1991).

Gosselin and Angeles (1988, 1989) considered isotropy of the Jacobian matrix for design optimization of planar and spherical three-DOF parallel manipulators. Arai et al. (1990) also used the Jacobian matrix in optimal design of a six-DOF parallel manipulator. Stiffness matrices of parallel manipulators, which are closely related to their Jacobian matrices, have been studied by Kerr (1989) and Gosselin (1990).

A class of three-limbed, six-DOF parallel minimanipulators were introduced by Tsai and Tahmasebi (1991a, 1991b) to obtain high positioning resolution and high stiffness in fine-manipulation operations.[1] In this paper, the Jacobian and stiffness matrices are derived for the minimanipulators. In addition, the Jacobian and stiffness matrices are used in establishing design guidelines for the minimanipulators.

2 DESCRIPTION OF THE MINIMANIPULATORS

Let subscript i in this section and the rest of this work represent numbers 1, 2, and 3 in a cyclic manner. A minimanipulator contains three inextensible limbs, P_iR_i, as shown in Figure 1. The lower end of each limb is connected to a two-DOF planar driver and can be moved freely on the base plate. The desired minimanipulator motion is obtained by moving the lower ends of its three limbs on its base plate. Two-DOF universal joints connect the limbs to the moving platform. The lower ends of the limbs are connected to the drivers through three more universal joints. Note that one of the axes of the upper universal joint is collinear with the limb, while the other axis of the upper universal joint as well as one of the axes of the lower universal

[1] A patent application has been filed for the minimanipulators.

This paper has been accepted for presentation at the 22nd ASME Biennial Mechanisms Conference (September 1992).

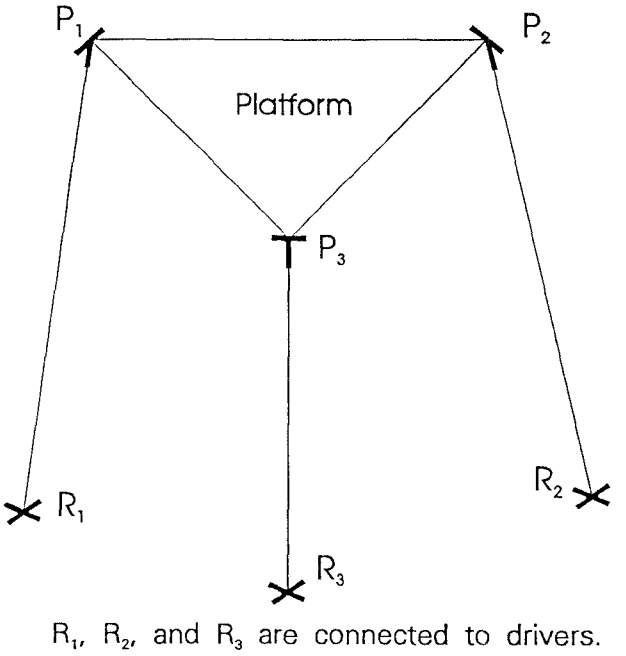

Figure 1: *Representation of a minimanipulator*

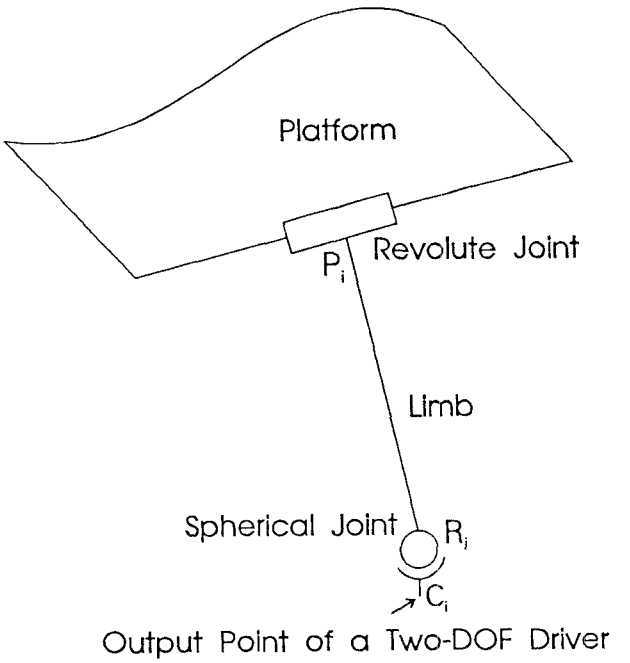

Figure 2: *Kinematic equivalent of a limb*

joint are always perpendicular to the limb. This arrangement is kinematically equivalent to a limb with a spherical joint at its lower end and a revolute joint at its upper end, as shown in Figure 2. In this paper, two types of minimanipulators are studied. The difference between Type 1 minimanipulators and Type 2 minimanipulators is in their two-DOF drivers.

In the Type 1 minimanipulator, bidirectional linear stepper motors (Yeaple, 1988) are used as drivers. Such stepper motors act as X-Y positioning tables, but their stators are base-mounted.

In the Type 2 minimanipulator, simplified five-bar linkage are used as drivers. Figure 3 shows drivers for the Type 2 minimanipulator. Point C_i is the output point of a driver. At point D_i, there is an actuator on each side of the base plate to drive links D_iA_i and D_iB_i. The simplified five-bar drivers are completely symmetric. That is

$$\left|\overline{D_iA_i}\right| = \left|\overline{D_iB_i}\right| = a \tag{1}$$

$$\left|\overline{A_iC_i}\right| = \left|\overline{B_iC_i}\right| = b \tag{2}$$

As a result, coordination between actuator rotations can be easily accomplished. Namely, angular displacement of an output point C_i is obtained by equal actuator rotations, and its radial displacement is obtained by equal and opposite actuator rotations.

Inextensible limbs and simplified five-bar linkages (in the Type 2 minimanipulator) are used to improve positional resolution and stiffness of a minimanipulator. Since the minimanipulator actuators are base-mounted; higher payload capacity, smaller actuator sizes, and lower power dissipation can be obtained. In addition, to achieve even load distribution, the minimanipulators are made completely symmetric. Namely, both triangles $D_1D_2D_3$ and $P_1P_2P_3$ are made equilateral and the joint axes at

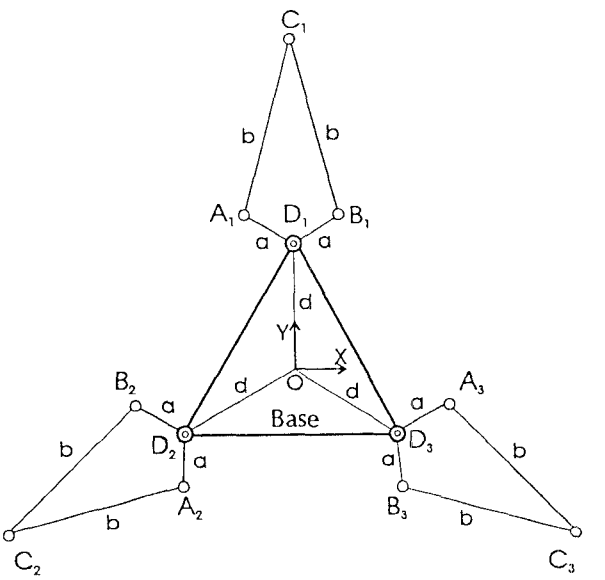

Figure 3: *Simplified five-bar linkage drivers*

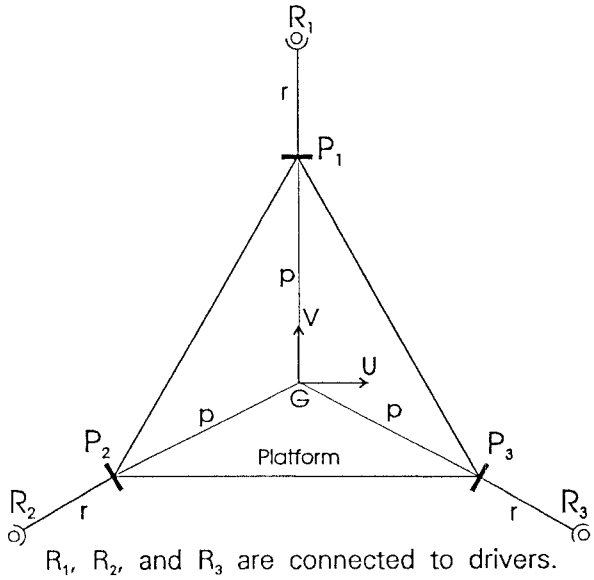

Figure 4: *Kinematic equivalent of a minimanipulator*

points P_1, P_2, and P_3 are made parallel to lines P_2P_3, P_1P_3, and P_1P_2, respectively.

In addition to the drivers mentioned above, other two-DOF mechanisms such as regular five-bar linkages, pantographs, or X-Y positioning tables can also be used as drivers for a minimanipulator (Tsai and Tahmasebi, 1991a).

3 TYPE 1 MINIMANIPULATOR

In this section, expressions for the Jacobian and stiffness matrices of the Type 1 minimanipulator are derived.

3.1 Jacobian Analysis

First, let us define a fixed reference frame (XYZ) and a moving reference frame (UVW). As shown in Figure 3, the fixed (or base) reference frame is attached to the base. The origin of the fixed reference frame (point O) is placed at the centroid of triangle $D_1D_2D_3$. The positive X-axis is parallel to and points in the direction of vector $\overline{D_2D_3}$. The positive Y-axis points from point O to point D_1. The Z-axis is defined by the right-hand-rule. The moving (or platform) reference frame is attached to the platform. The origin of the moving reference frame (point G) is placed at the centroid of triangle $P_1P_2P_3$ (see Figure 4). The positive U-axis is parallel to and points in the direction of vector $\overline{P_2P_3}$. The positive V-axis points from point O to point P_1. The W-axis is defined by the right-hand-rule.

In this paper, without loss of generality, we let $Z_{R,i} = 0$. If $Z_{R,i} > 0$ for a minimanipulator, a simple transformation should be applied to the coordinates of the points used in the following derivations.

Referring to Figure 5, we can write the following vector equation

$$\overline{OR_i} = \overline{OG} + \overline{GP_i} + \overline{P_iR_i} \tag{3}$$

Taking the time derivative of both sides of equation (3) with respect to the fixed reference frame yields

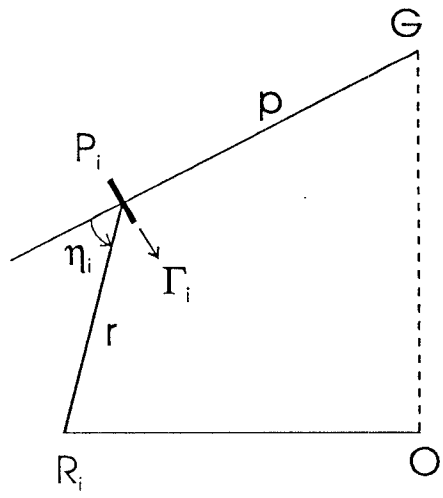

Figure 5: *Parameters used in Jacobian analysis*

$$^B\overline{V}^{R_i} = {}^B\overline{V}^G + {}^B\overline{\omega}^P \times \overline{GP_i} + {}^B\overline{\omega}^{L_i} \times \overline{P_iR_i} \tag{4}$$

where $\overline{V}$ and $\overline{\omega}$ denote linear and angular velocities, respectively. The right superscript for a velocity vector stands for a point or a rigid body, whereas the left superscript refers to a reference frame in which the velocity is expressed. The base, the platform, and limb $\overline{P_iR_i}$ reference frames (rigid bodies) are denoted by B, P, and L_i, respectively. The terms rigid body and reference frame are used interchangeably, because every rigid body can be used as a reference frame and every reference frame can be viewed as a massless rigid body (Kane and Levinson, 1985). Angular velocity of limb $\overline{P_iR_i}$ in the fixed reference frame can be found from

$$^B\overline{\omega}^{L_i} = {}^P\overline{\omega}^{L_i} + {}^B\overline{\omega}^P \tag{5}$$

As shown in Figure 5, let η_i be the angle from vector $\overline{GP_i}$ to vector $\overline{P_iR_i}$ measured about a unit vector $\overline{\Gamma}_i$ which is collinear with the axis of the revolute joint at point P_i and points in the direction of vector $\overline{P_{i+2}P_{i+1}}$. [2] Then

$$^B\overline{\omega}^{L_i} = \dot{\eta}_i\overline{\Gamma}_i + {}^B\overline{\omega}^P \tag{6}$$

where $\dot{\eta}_i$ is the time-derivative of η_i. Substituting the above expression for $^B\overline{\omega}^{L_i}$ in equation (4), and simplifying, we obtain

$$^B\overline{V}^{R_i} = {}^B\overline{V}^G + {}^B\overline{\omega}^P \times \overline{GR_i} + \dot{\eta}_i\overline{\Gamma}_i \times \overline{P_iR_i} \tag{7}$$

The Z-component of $^B\overline{V}^{R_i}$ is equal to zero. Therefore, we can conclude from the above equation that

$$\dot{\eta}_i = -\frac{{}^B\overline{V}^G \cdot \bar{n}_z + ({}^B\overline{\omega}^P \times \overline{GR_i}) \cdot \bar{n}_z}{(\overline{\Gamma}_i \times \overline{P_iR_i}) \cdot \bar{n}_z} \tag{8}$$

where $\bar{n}_z$ is a unit vector in the Z-direction. Let

$$\overline{\mu}_i = \overline{\Gamma}_i \times \overline{P_iR_i} \tag{9}$$

[2] The subscripts are cyclic, with a cycle length of 3.

Then, equation (8) reduces to

$$\dot{\eta}_i = -\frac{\bar{n}_z \cdot {}^B\overline{V}^G + (\overline{GR_i} \times \bar{n}_z) \cdot {}^B\overline{\omega}^P}{\mu_{i,z}} \tag{10}$$

where $\mu_{i,z}$ is the Z-component of the vector $\overline{\mu}_i$. Also, let

$$\mu'_{i,x} = \frac{\mu_{i,x}}{\mu_{i,z}} \quad , \quad \mu'_{i,y} = \frac{\mu_{i,y}}{\mu_{i,z}}$$

where $\mu_{i,x}$ and $\mu_{i,y}$ are the X and Y-components of vector $\overline{\mu}_i$, respectively. Substituting equation (10) into equation (7), and solving for the X-component of the resulting equation, we obtain

$$\begin{aligned} {}^B V_x^{R_i} &= (\bar{n}_x - \mu'_{i,x}\bar{n}_z) \cdot {}^B\overline{V}^G + \\ &\quad [(\overline{GR_i} \times \bar{n}_x) - \mu'_{i,x}(\overline{GR_i} \times \bar{n}_z)] \cdot {}^B\overline{\omega}^P \end{aligned} \tag{11}$$

where ${}^B V_x^{R_i}$ is the X-component of vector ${}^B\overline{V}^{R_i}$ and $\bar{n}_x$ is a unit vector in the X-direction. Similarly, we can obtain the following equation

$$\begin{aligned} {}^B V_y^{R_i} &= (\bar{n}_y - \mu'_{i,y}\bar{n}_z) \cdot {}^B\overline{V}^G + \\ &\quad [(\overline{GR_i} \times \bar{n}_y) - \mu'_{i,y}(\overline{GR_i} \times \bar{n}_z)] \cdot {}^B\overline{\omega}^P \end{aligned} \tag{12}$$

where ${}^B V_y^{R_i}$ is the Y-component of vector ${}^B\overline{V}^{R_i}$ and $\bar{n}_y$ is a unit vector in the Y-direction.

Let us define the 6×1 twist vector of the platform ($\dot{\overline{x}}$) as

$$\dot{\overline{x}} = \begin{bmatrix} {}^B\overline{V}^G \\ {}^B\overline{\omega}^P \end{bmatrix} \tag{13}$$

If the 6×1 vector of velocity components at the lower ends of the limbs ($\dot{\overline{q}}$) is given by

$$\dot{\overline{q}} = [{}^B\overline{V}_x^{R_1}, \ {}^B\overline{V}_y^{R_1}, \ {}^B\overline{V}_x^{R_2}, \ {}^B\overline{V}_y^{R_2}, \ {}^B\overline{V}_x^{R_3}, \ {}^B\overline{V}_y^{R_3}]^T \tag{14}$$

Then, we can define the 6×6 Jacobian matrix ($\mathbf{J}$) by

$$\dot{\overline{q}} = \mathbf{J}\dot{\overline{x}} \tag{15}$$

Referring to equations (11) and (12), we can express the Jacobian matrix as

$$\mathbf{J} = \begin{bmatrix} (\bar{n}_x - \mu'_{1,x}\bar{n}_z)^T & [(\overline{GR_1} \times \bar{n}_x) - \mu'_{1,x}(\overline{GR_1} \times \bar{n}_z)]^T \\ (\bar{n}_y - \mu'_{1,y}\bar{n}_z)^T & [(\overline{GR_1} \times \bar{n}_y) - \mu'_{1,y}(\overline{GR_1} \times \bar{n}_z)]^T \\ (\bar{n}_x - \mu'_{2,x}\bar{n}_z)^T & [(\overline{GR_2} \times \bar{n}_x) - \mu'_{2,x}(\overline{GR_2} \times \bar{n}_z)]^T \\ (\bar{n}_y - \mu'_{2,y}\bar{n}_z)^T & [(\overline{GR_2} \times \bar{n}_y) - \mu'_{2,y}(\overline{GR_2} \times \bar{n}_z)]^T \\ (\bar{n}_x - \mu'_{3,x}\bar{n}_z)^T & [(\overline{GR_3} \times \bar{n}_x) - \mu'_{3,x}(\overline{GR_3} \times \bar{n}_z)]^T \\ (\bar{n}_y - \mu'_{3,y}\bar{n}_z)^T & [(\overline{GR_3} \times \bar{n}_y) - \mu'_{3,y}(\overline{GR_3} \times \bar{n}_z)]^T \end{bmatrix} \tag{16}$$

where superscript T denotes transpose.

Note that due to dualities of parallel and serial manipulators (Waldron and Hunt, 1987), we have defined the Jacobian matrix as the transformation which maps the Cartesian velocities to joint rates. This is a common practice among most researchers who have studied parallel manipulators (e.g.; Gosselin and Angeles, 1988, 1989; Gosselin, 1990; Arai et al., 1990).

3.2 Stiffness Analysis

From equation (15), we can conclude that

$$\overline{\delta q} = \mathbf{J}\overline{\delta x} \tag{17}$$

where $\overline{\delta q}$ and $\overline{\delta x}$ represent infinitesimal displacements at the lower ends of the limbs and at the center of the platform, respectively. Equation (15) and the principle of virtual work can be used to derive the following equation (Asada and Slotine, 1986).

$$\overline{\mathcal{F}} = \mathbf{J}^T\overline{f} \tag{18}$$

where

$$\overline{\mathcal{F}} = \begin{bmatrix} \overline{F}_P \\ \overline{M}_P \end{bmatrix} \tag{19}$$

and

$$\overline{f} = [f_{1,x}, \ f_{1,y}, \ f_{2,x}, \ f_{2,y}, \ f_{3,x}, \ f_{3,y}]^T \tag{20}$$

Vectors $\overline{F}_P$ and $\overline{M}_P$ in equation (19) represent the force and moment applied to the platform. Also, $f_{i,x}$ and $f_{i,y}$ in equation (20) are the X and Y-components of the actuator force applied at point R_i. The actuator forces and displacements at the lower ends of the limbs can be related by the following equation.

$$\overline{f} = \mathrm{k}\overline{\delta q} \tag{21}$$

where k is a 6×6 diagonal matrix whose elements have units of force per unit length. Substituting equation (17) into equation (21) and the resulting equation into equation (18), yields

$$\overline{\mathcal{F}} = \mathbf{J}^T\mathrm{k}\mathbf{J}\overline{\delta x} \tag{22}$$

If k represents the stiffness of each bilinear stepper motor (actuator) in the X and Y directions, then the diagonal elements of k are all equal to k. Therefore, the stiffness matrix for the platform ($\mathbf{K}$) can be expressed as

$$\mathrm{K} = k\mathbf{J}^T\mathbf{J} \tag{23}$$

Note that $\mathbf{K}$ is a symmetric, positive semidefinite matrix. Elements of the lower triangular portion of $\mathbf{K}/k$ ($\check{\mathrm{K}}$) are given in Appendix A.

3.3 Central Stiffness Matrix

In this subsection, the stiffness matrix at the central configuration of the minimanipulator workspace (central stiffness matrix) will be derived. The central configuration is defined as the configuration where

1. The platform is not rotated with respect to the base.
2. The centroid of triangle $P_1P_2P_3$ (platform) is directly on top of the centroid of triangle $D_1D_2D_3$, i.e. $X_G = Y_G = 0$.

Let $\left|\overline{GP_i}\right| = p$. Also, at the central configuration , let $\left|\overline{OR_i}\right| = \nu$ and $Z_G = \zeta$. Using equations (16) and (23), the stiffness matrix at the central configuration (K^+) is found to be

$$\mathrm{K}^+ = 3k \begin{bmatrix} 1 & 0 & 0 & 0 & \frac{(2p-\nu)\zeta}{2(\nu-p)} & 0 \\ 0 & 1 & 0 & \frac{(\nu-2p)\zeta}{2(\nu-p)} & 0 & 0 \\ 0 & 0 & \frac{\zeta^2}{(\nu-p)^2} & 0 & 0 & 0 \\ 0 & \frac{(\nu-2p)\zeta}{2(\nu-p)} & 0 & \frac{(\nu^2-2p\nu+2p^2)\zeta^2}{2(\nu-p)^2} & 0 & 0 \\ \frac{(2p-\nu)\zeta}{2(\nu-p)} & 0 & 0 & 0 & \frac{(\nu^2-2p\nu+2p^2)\zeta^2}{2(\nu-p)^2} & 0 \\ 0 & 0 & 0 & 0 & 0 & \nu^2 \end{bmatrix} \tag{24}$$

It is desirable to eliminate the off-diagonal terms which couple the forces (moments) applied along (about) the X and Y axes to the rotations (translations) about (along) the Y and X axes, respectively. Fortunately, this can be easily accomplished by setting

$$p = \frac{\nu}{2} \tag{25}$$

In other words, the platform (triangle $P_1P_2P_3$) should be one-half of triangle $R_1R_2R_3$ at the central configuration. The above result is similar to that obtained by Kerr (1989) in designing a Stewart-platform-based force and torque transducer. If the condition expressed in the above equation is satisfied, then

$$\zeta^2 = r^2 - p^2 \tag{26}$$

where r is the length of any limb. If equations (25) and (26) are used to substitute for ν and ζ in equation (24), matrix $\mathbf{K}^+$ reduces to

$$\mathbf{K}^* = 3k \begin{bmatrix} 1 & & & & & 0 \\ & 1 & & & & \\ & & (r^2-p^2)/p^2 & & & \\ & & & r^2-p^2 & & \\ & & & & r^2-p^2 & \\ & & 0 & & & 4p^2 \end{bmatrix} \tag{27}$$

The above equation can be used to determine the relative dimensions of the minimanipulator so that desirable characteristics can be obtained. Note that dimension ν (the independent variable) can be determined from other requirements and constraints such as maximizing the workspace and the upper bound on size of the base plate.

For some applications, it may be desirable to maximize one or more of the diagonal elements of $\mathbf{K}^*$ ($K^*_{1,1}, K^*_{2,2}, \ldots, K^*_{6,6}$). For other applications, the designer may be interested in isotropic stiffness properties. Note that it is not possible to make all of the diagonal stiffness terms equal to one another. However, it will be shown that it is possible to obtain isotropic direct stiffness or isotropic torsional stiffness.

To move the platform in the X or Y-direction, the lower ends of all three limbs should also move in the X or Y-direction. As a result, elements $K^*_{1,1}$ and $K^*_{2,2}$ are constants. Element $K^*_{3,3}$ is proportional to tangent-squared of the angle between any of the limbs and the base plane. The closer this angle to 90 degrees, the larger the direct stiffness in the Z-direction. Stiffness terms $K^*_{3,3}, K^*_{4,4}$, and $K^*_{5,5}$ are functions of two design variables (r and p). However, $K^*_{6,6}$ is only dependent on variable p (circumradius of the platform). This is related to the fact that in order to rotate the platform about the Z-axis, the lower ends of the limbs should move on a circle, which passes through them, in the same direction and by an equal amount.

The first three diagonal terms of the $\mathbf{K}^*$ matrix are direct stiffness terms. Equation (27) shows that by setting

$$r = \sqrt{2}p$$

we can obtain equal direct stiffness values in the X, Y, and Z directions. At this configuration, the angle between any of the limbs and the base plane becomes equal to 45 degrees.

The last three diagonal terms of the $\mathbf{K}^*$ matrix are torsional stiffness terms. Referring to equation (27), we notice that by setting

$$r = \sqrt{5}p$$

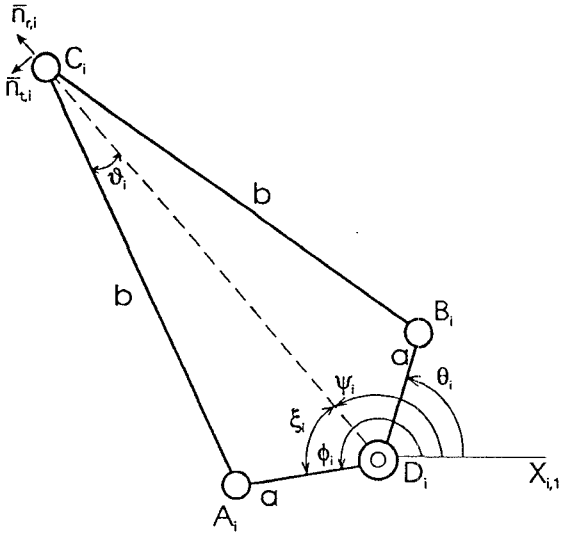

Figure 6: *Parameters used in velocity analysis of drivers*

we can obtain equal torsional stiffness values in the X, Y, and Z directions. At this configuration, the angle between any of the limbs and the base plane becomes equal to 63.43 degrees.

4 TYPE 2 MINIMANIPULATOR

In this section, expressions for the Jacobian and stiffness matrices of the Type 2 minimanipulator are derived.

4.1 Jacobian Analysis

Figure 6 shows a simplified five-bar driver. Let θ_i and ϕ_i (driver input angles) be the angles from the positive X-axis to the vectors $\overline{D_iB_i}$ and $\overline{D_iA_i}$, respectively, measured about the positive Z-axis. D_iB_i and D_iA_i are the input links of the driver and vector $\overline{D_iX_{i,1}}$ is parallel to the positive X-axis. In the following analysis, we assume that $\phi_i \geq \theta_i$ (if $\phi_i < \theta_i$, 360 degrees is added to ϕ_i). In addition, only one branch of a driver is considered, because the other branch can be realized only by disassembling and reassembling the driver. From the driver geometry, we can write

$$\left|\overline{D_iC_i}\right| = a\cos\xi_i + b\cos\vartheta_i \tag{28}$$

where ξ_i is the angle of line D_iC_i with line D_iB_i or line D_iA_i and ϑ_i is the angle of line C_iD_i with line C_iB_i or line C_iA_i. Applying the law of sines to triangle $D_iA_iC_i$, we get

$$\frac{\sin\vartheta_i}{a} = \frac{\sin\xi_i}{b} \tag{29}$$

or

$$\cos\vartheta_i = \sqrt{1-(a/b)^2\sin^2\xi_i} \tag{30}$$

From equations (28) and (30), we conclude that

$$\overline{D_iC_i} = \left[a\cos\xi_i + b\sqrt{1-(a/b)^2\sin^2\xi_i}\right]\bar{n}_{r,i} \tag{31}$$

where $\bar{n}_{r,i}$ is a unit vector in the direction of vector $\overline{D_iC_i}$.

Let ψ_i be the angle from the positive X-axis to the vector $\overline{D_iC_i}$, measured about the positive Z-axis. Also, as shown in Figure 6, let the unit vector $\bar{n}_{t,i}$ be at 90 degrees to the unit vector $\bar{n}_{r,i}$, measured about the positive Z-axis. Taking the time-derivative of both sides of equation (31), with respect to the fixed reference frame, we obtain

$$\begin{bmatrix} {}^{B}V_r^{C_i} \\ {}^{B}V_t^{C_i} \end{bmatrix} = \Delta^{(i)} \begin{bmatrix} \dot{\xi}_i \\ \dot{\psi}_i \end{bmatrix} \tag{32}$$

where $\Delta^{(i)}$ is a 2×2 diagonal matrix whose diagonal elements are given by

$$\Delta_{1,1}^{(i)} = -b\left[(a/b)\sin\xi_i + (a/b)^2 \frac{\sin\xi_i \cos\xi_i}{\sqrt{1-(a/b)^2\sin^2\xi_i}}\right] \tag{33}$$

$$\Delta_{2,2}^{(i)} = b\left[(a/b)\cos\xi_i + \sqrt{1-(a/b)^2\sin^2\xi_i}\right] \tag{34}$$

and $({}^{B}V_r^{C_i}, {}^{B}V_t^{C_i})$ are the radial (in the $\bar{n}_{r,i}$ direction) and tangential (in the $\bar{n}_{t,i}$ direction) components of the velocity of point C_i. In addition, $\dot{\xi}_i$ and $\dot{\psi}_i$ denote time-derivatives of angles ξ_i and ψ_i, respectively. Note that $\dot{\xi}_i$ and $\dot{\psi}_i$ are related to the input speeds ($\dot{\theta}_i$ and $\dot{\phi}_i$) by the following linear relationships.

$$\dot{\psi}_i = (\dot{\phi}_i + \dot{\theta}_i)/2 \tag{35}$$

$$\dot{\xi}_i = (\dot{\phi}_i - \dot{\theta}_i)/2 \tag{36}$$

Equations (32) - (36) show that for a given b, the smaller the ratio a/b, the higher the speed reduction (mechanical advantage) of the driver in the radial direction.

Substituting equations (35) and (36) into equation (32), and simplifying, we obtain

$$\begin{bmatrix} \dot{\theta}_i \\ \dot{\phi}_i \end{bmatrix} = \begin{bmatrix} -1/\Delta_{1,1}^{(i)} & 1/\Delta_{2,2}^{(i)} \\ 1/\Delta_{1,1}^{(i)} & 1/\Delta_{2,2}^{(i)} \end{bmatrix} \begin{bmatrix} {}^{B}V_r^{C_i} \\ {}^{B}V_t^{C_i} \end{bmatrix} \tag{37}$$

We can also write

$$\begin{bmatrix} {}^{B}V_r^{C_i} \\ {}^{B}V_t^{C_i} \end{bmatrix} = \begin{bmatrix} C\psi_i & S\psi_i \\ -S\psi_i & C\psi_i \end{bmatrix} \begin{bmatrix} {}^{B}V_x^{C_i} \\ {}^{B}V_y^{C_i} \end{bmatrix} \tag{38}$$

where $({}^{B}V_x^{C_i}, {}^{B}V_y^{C_i})$ are the components of the velocity of point C_i in the X and Y directions, respectively; $C\psi_i = \cos\psi_i$; and $S\psi_i = \sin\psi_i$. Equations (37) and (38) imply that

$$\begin{bmatrix} \dot{\theta}_i \\ \dot{\phi}_i \end{bmatrix} = \mathbf{J_d}^{(i)} \begin{bmatrix} {}^{B}V_x^{C_i} \\ {}^{B}V_y^{C_i} \end{bmatrix} \tag{39}$$

where

$$\mathbf{J_d}^{(i)} = \begin{bmatrix} -C\psi_i/\Delta_{1,1}^{(i)} - S\psi_i/\Delta_{2,2}^{(i)} & -S\psi_i/\Delta_{1,1}^{(i)} + C\psi_i/\Delta_{2,2}^{(i)} \\ C\psi_i/\Delta_{1,1}^{(i)} - S\psi_i/\Delta_{2,2}^{(i)} & S\psi_i/\Delta_{1,1}^{(i)} + C\psi_i/\Delta_{2,2}^{(i)} \end{bmatrix} \tag{40}$$

Let $\dot{\bar{\theta}}$ be the 6×1 vector of input joint rates, i.e.

$$\dot{\bar{\theta}} = [\dot{\theta}_1,\ \dot{\phi}_1,\ \dot{\theta}_2,\ \dot{\phi}_2,\ \dot{\theta}_3,\ \dot{\phi}_3]^T \tag{41}$$

Since ${}^{B}V_x^{R_i} = {}^{B}V_x^{C_i}$ and ${}^{B}V_y^{R_i} = {}^{B}V_y^{C_i}$, we can write

$$\dot{\bar{\theta}} = \mathbf{J_d}\dot{\bar{q}} \tag{42}$$

where $\dot{\bar{q}}$ is defined in equation (14) and $\mathbf{J_d}$ is the 6×6 Jacobian for the drivers which is given by

$$\mathbf{J_d} = \begin{bmatrix} \mathbf{J_d}^{(1)} & & \mathbf{0} \\ & \mathbf{J_d}^{(2)} & \\ \mathbf{0} & & \mathbf{J_d}^{(3)} \end{bmatrix} \tag{43}$$

The overall Jacobian for a Type 2 minimanipulator ($\hat{\mathbf{J}}$) is defined by

$$\dot{\bar{\theta}} = \hat{\mathbf{J}}\dot{\bar{x}} \tag{44}$$

where $\dot{\bar{x}}$ is defined in equation (13). Referring to equations (15) and (42), we can see that

$$\hat{\mathbf{J}} = \mathbf{J_d}\mathbf{J} \tag{45}$$

where $\mathbf{J}$, which can be found from equation (16), represents the Jacobian for the main portion (platform and limbs) of the minimanipulator.

4.2 Stiffness Analysis

Equation (44) implies that

$$\overline{\delta\theta} = \hat{\mathbf{J}}\overline{\delta x} \tag{46}$$

where $\overline{\delta\theta}$ and $\overline{\delta x}$ represent infinitesimal displacements of the actuated joints and the platform, respectively. Let $\bar{\tau}$ be the 6×1 vector of input joint torques. Similar to equation (18), we can write

$$\overline{\mathcal{F}} = \hat{\mathbf{J}}^T\bar{\tau} \tag{47}$$

where $\overline{\mathcal{F}}$ is defined in equation (19). Input actuator torques and displacements are related by

$$\bar{\tau} = \hat{\mathrm{k}}\overline{\delta\theta} \tag{48}$$

where $\hat{\mathrm{k}}$ is a 6×6 diagonal matrix whose elements represent stiffness of the actuators. Substituting equation (46) into equation (48) and the resulting equation into equation (47), yields

$$\overline{\mathcal{F}} = \hat{\mathbf{J}}^T\hat{\mathrm{k}}\hat{\mathbf{J}}\overline{\delta x} \tag{49}$$

The above equation and equation (45) show that the stiffness matrix for the platform ($\hat{\mathrm{K}}$) is given by

$$\hat{\mathrm{K}} = \hat{\mathbf{J}}^T\hat{\mathrm{k}}\hat{\mathbf{J}} = \mathbf{J}^T{\mathbf{J_d}}^T\hat{\mathrm{k}}\mathbf{J_d}\mathbf{J} \tag{50}$$

5 DESIGN GUIDELINES

Based on the results of subsection 3.3, the following design guidelines can be established for the Type 1 minimanipulator.

- The central stiffness matrix can be diagonalized (decoupled) by making the platform (triangle $P_1P_2P_3$) one-half the size of the triangle passing through the lower ends of the limbs, i.e. $p = \nu/2$.
- If the central stiffness matrix is decoupled, then
  - Direct stiffness isotropy can be obtained by making the limb length equal to $\sqrt{2}$ times the circumradius of the platform, i.e. $r = \sqrt{2}p$.
  - Torsional stiffness isotropy can be obtained by making the limb length equal to $\sqrt{5}$ times the circumradius of the platform, i.e. $r = \sqrt{5}p$.

- The larger the ratio of the limb length to the platform circumradius (r/p), the larger the direct stiffness in the Z-direction.
- For a given platform size, the larger the limb length, the larger the torsional stiffness values in the X and Y-directions.
- For a given limb length, the larger the platform size, the smaller the torsional stiffness values in the X and Y-directions, and the larger the torsional stiffness in the Z-direction.

Note that a minimanipulator will be at or near the center of its workspace during most of its operations. Therefore, establishing design guidelines based on the central stiffness matrix is justified.

The main portion (platform and limbs) of the Type 2 minimanipulator is the same as that of the Type 1 minimanipulator. Therefore, the above design guidelines can also be applied to the Type 2 minimanipulator. In addition, based on the results of subsection 4.1, the following design guideline can be established for the five-bar drivers of the Type 2 minimanipulator.

- The smaller the ratio of the input link length to the output link length of a driver (a/b), the higher the stiffness of the minimanipulator.

6 SUMMARY

In this paper, the Jacobian and stiffness matrices of two types of three-limbed, six-DOF parallel minimanipulators are derived. It is shown that the stiffness matrix at the central configuration of a Type 1 minimanipulator workspace can be decoupled, if the platform size is made half of the size of the triangle passing through the lower ends of the limbs. It is also shown that, at the central configuration of a Type 1 minimanipulator, ratio of the limb length to the platform circumradius must be equal to $\sqrt{2}$ ($\sqrt{5}$) for obtaining direct (torsional) stiffness isotropy. Finally, guidelines for obtaining high stiffness values and for designing drivers of the Type 2 minimanipulator are established.

ACKNOWLEDGMENTS

This research was supported in part by the U.S. Department of Energy under Grant DEF05-88ER13977 and in part by the NSF Engineering Research Centers program, NSFD CDR 8803012. The first author gratefully acknowledges the support of NASA/Goddard Space Flight Center. Such supports do not constitute endorsements of the views expressed in the paper by the supporting agencies.

REFERENCES

- Arai, T., Cleary, K., Nakamura, T., Adachi, H., and Homma, K., 1990, "Design, Analysis and Construction of a Prototype Parallel Link Manipulator," *Proc. of the IEEE International Workshop on Intelligent Robots and Systems (IROS '90)*, pp. 205-212.
- Asada, H., and Slotine, J.-J.E., 1986, *Robot Analysis and Control*, John Wiley and Sons, New York.
- Fichter, E.F., 1986, "A Stewart Platform-based Manipulator: General Theory and Practical Construction," *Int. J. of Robotics Research*, Vol. 5, pp. 157-182.
- Gosselin, C., and Angeles, J., 1988, "The Optimum Kinematic Design of a Planar Three-Degree-of-Freedom Parallel Manipulator," *Trans. ASME, J. of Mech., Transmis., and Auto. in Design*, Vol. 110, pp. 35-41.
- Gosselin, C., and Angeles, J., 1989, "The Optimum Kinematic Design of a Spherical Three-Degree-of-Freedom Parallel Manipulator," *Trans. ASME, J. of Mech., Transmis., and Auto. in Design*, Vol. 111, pp. 202-207.
- Gosselin, C., 1990, "Stiffness Mapping of Parallel Manipulators," *IEEE Transactions on Robotics and Automation*, Vol. 6, pp. 377-382.
- Griffis, M., and Duffy, J., 1989, "A Forward Displacement Analysis of a Class of Stewart Platforms," *J. of Robotic Systems*, Vol. 6, pp. 703-720.
- Hudgens, J.C., and Tesar, D., 1988, "A Fully-Parallel Six Degree-of-Freedom Micromanipulator: Kinematic Analysis and Dynamic Model," *Trends and Developments in Mechanisms, Machines, and Robotics - Proc. of the 20th Biennial Mechanisms Conference*, ASME, New York, DE-Vol. 15-3, pp. 29-37.
- Hunt, K.H., 1983, "Structural Kinematics of In-Parallel-Actuated Robot-Arms," *Trans. ASME, J. of Mech., Transmis., and Auto. in Design*, Vol. 105, pp. 705-712.
- Innocenti, C., and Parenti-Castelli, V., 1990, "Direct Position Analysis of the Stewart Platform Mechanism," *Mechanism and Machine Theory*, Vol. 25, pp. 611-612.
- Kane, T.R., and Levinson, D.A., 1985, *Dynamics: Theory and Applications*, McGraw-Hill, New York.
- Kerr, D.R., 1989, "Analysis, Properties, and Design of a Stewart-Platform Transducer," *Trans. ASME, J. of Mech., Transmis., and Auto. in Design*, Vol. 111, pp. 25-28.
- Kohli, D., Lee, S.H., Tsai, K.Y., and Sandor, G.N., 1988, "Manipulator Configurations Based on Rotary-Linear (R-L) Actuators and Their Direct and Inverse Kinematics," *Trans. ASME, J. of Mech., Transmis., and Auto. in Design*, Vol. 110, pp. 397-404.
- Nanua, P., Waldron, K.J., and Murthy, V., 1990, "Direct Kinematic Solution of a Stewart Platform," *IEEE Transactions on Robotics and Automation*, Vol. 6, pp. 438-444.
- Stewart, D., 1965, "A Platform with Six Degrees of Freedom," *Proc. Institute of Mechanical Engr.*, London, England, Vol. 180, pp. 371-386.
- Tahmasebi, F., and Tsai, L.W., 1991, "Closed-Form Direct Kinematics Solution of a New Parallel Minimanipulator," *Technical Research Report TR 91-92*, Systems Research Center, University of Maryland, College Park.

- Tsai, L.W., and Tahmasebi, F., 1991a, "Synthesis and Analysis of a New Class of Six-Degree-of-Freedom Parallel Minimanipulators," *Technical Research Report TR 91-83*, Systems Research Center, University of Maryland, College Park.
- Tsai, L.W., and Tahmasebi, F., 1991b, "Design and Analysis of a New Six-Degree-of-Freedom Parallel Minimanipulator," *Proc. of the 6th International Conference on CAD/CAM, Robotics, and Factories of the Future* , Springer-Verlag, Berlin.
- Waldron, K.J., and Hunt, K.H., 1987, "Series-Parallel Dualities in Actively Coordinated Mechanisms," *Proc. of the 4th Int. Symp. on Robotic Research*, MIT press, Cambridge, MA, pp. 175-181.
- Yeaple, F., 1988, "Choreographed Robots Insert Automotive Parts," *Design News*, Vol. 44, No. 21, pp. 134-135.

APPENDIX A - LOWER TRIANGULAR ELEMENTS OF $\check{K}$

$$\check{K}_{1,1} = 3$$

$$\check{K}_{2,1} = 0$$

$$\check{K}_{2,2} = 3$$

$$\check{K}_{3,1} = -\mu'_{3,x} - \mu'_{2,x} - \mu'_{1,x}$$

$$\check{K}_{3,2} = -\mu'_{3,y} - \mu'_{2,y} - \mu'_{1,y}$$

$$\check{K}_{3,3} = {\mu'_{3,y}}^2 + {\mu'_{3,x}}^2 + {\mu'_{2,y}}^2 + {\mu'_{2,x}}^2 + {\mu'_{1,y}}^2 + {\mu'_{1,x}}^2$$

$$\check{K}_{4,1} = -\mu'_{3,x}(Y_{R,3} - Y_G) - \mu'_{2,x}(Y_{R,2} - Y_G) - \mu'_{1,x}(Y_{R,1} - Y_G)$$

$$\check{K}_{4,2} = 3Z_G - \mu'_{3,y}(Y_{R,3} - Y_G) - \mu'_{2,y}(Y_{R,2} - Y_G) - \mu'_{1,y}(Y_{R,1} - Y_G)$$

$$\check{K}_{4,3} = -\mu'_{3,y}[Z_G - \mu'_{3,y}(Y_{R,3} - Y_G)] - \mu'_{2,y}[Z_G - \mu'_{2,y}(Y_{R,2} - Y_G)] - \mu'_{1,y}[Z_G - \mu'_{1,y}(Y_{R,1} - Y_G)] + {\mu'_{3,x}}^2(Y_{R,3} - Y_G) + {\mu'_{2,x}}^2(Y_{R,2} - Y_G) + {\mu'_{1,x}}^2(Y_{R,1} - Y_G)$$

$$\check{K}_{4,4} = [Z_G - \mu'_{3,y}(Y_{R,3} - Y_G)]^2 + [Z_G - \mu'_{2,y}(Y_{R,2} - Y_G)]^2 + [Z_G - \mu'_{1,y}(Y_{R,1} - Y_G)]^2 + {\mu'_{3,x}}^2(Y_{R,3} - Y_G)^2 + {\mu'_{2,x}}^2(Y_{R,2} - Y_G)^2 + {\mu'_{1,x}}^2(Y_{R,1} - Y_G)^2$$

$$\check{K}_{5,1} = -3Z_G - \mu'_{3,x}(X_G - X_{R,3}) - \mu'_{2,x}(X_G - X_{R,2}) - \mu'_{1,x}(X_G - X_{R,1})$$

$$\check{K}_{5,2} = -\mu'_{3,y}(X_G - X_{R,3}) - \mu'_{2,y}(X_G - X_{R,2}) - \mu'_{1,y}(X_G - X_{R,1})$$

$$\check{K}_{5,3} = -\mu'_{3,x}[-Z_G - \mu'_{3,x}(X_G - X_{R,3})] - \mu'_{2,x}[-Z_G - \mu'_{2,x}(X_G - X_{R,2})] - \mu'_{1,x}[-Z_G - \mu'_{1,x}(X_G - X_{R,1})] + {\mu'_{3,y}}^2(X_G - X_{R,3}) + {\mu'_{2,y}}^2(X_G - X_{R,2}) + {\mu'_{1,y}}^2(X_G - X_{R,1})$$

$$\check{K}_{5,4} = -\mu'_{3,y}(X_G - X_{R,3})[Z_G - \mu'_{3,y}(Y_{R,3} - Y_G)] - \mu'_{2,y}(X_G - X_{R,2})[Z_G - \mu'_{2,y}(Y_{R,2} - Y_G)] - \mu'_{1,y}(X_G - X_{R,1})[Z_G - \mu'_{1,y}(Y_{R,1} - Y_G)] - \mu'_{3,x}(Y_{R,3} - Y_G)[-Z_G - \mu'_{3,x}(X_G - X_{R,3})] - \mu'_{2,x}(Y_{R,2} - Y_G)[-Z_G - \mu'_{2,x}(X_G - X_{R,2})] - \mu'_{1,x}(Y_{R,1} - Y_G)[-Z_G - \mu'_{1,x}(X_G - X_{R,1})]$$

$$\check{K}_{5,5} = [-Z_G - \mu'_{3,x}(X_G - X_{R,3})]^2 + [-Z_G - \mu'_{2,x}(X_G - X_{R,2})]^2 + [-Z_G - \mu'_{1,x}(X_G - X_{R,1})]^2 + {\mu'_{3,y}}^2(X_G - X_{R,3})^2 + {\mu'_{2,y}}^2(X_G - X_{R,2})^2 + {\mu'_{1,y}}^2(X_G - X_{R,1})^2$$

$$\check{K}_{6,1} = -Y_{R,3} - Y_{R,2} - Y_{R,1} + 3Y_G$$

$$\check{K}_{6,2} = X_{R,3} + X_{R,2} + X_{R,1} - 3X_G$$

$$\check{K}_{6,3} = -\mu'_{3,x}(Y_G - Y_{R,3}) - \mu'_{2,x}(Y_G - Y_{R,2}) - \mu'_{1,x}(Y_G - Y_{R,1}) - \mu'_{3,y}(X_{R,3} - X_G) - \mu'_{2,y}(X_{R,2} - X_G) - \mu'_{1,y}(X_{R,1} - X_G)$$

$$\check{K}_{6,4} = (X_{R,3} - X_G)[Z_G - \mu'_{3,y}(Y_{R,3} - Y_G)] + (X_{R,2} - X_G)[Z_G - \mu'_{2,y}(Y_{R,2} - Y_G)] + (X_{R,1} - X_G)[Z_G - \mu'_{1,y}(Y_{R,1} - Y_G)] - \mu'_{3,x}(Y_G - Y_{R,3})(Y_{R,3} - Y_G) - \mu'_{2,x}(Y_G - Y_{R,2})(Y_{R,2} - Y_G) - \mu'_{1,x}(Y_G - Y_{R,1})(Y_{R,1} - Y_G)$$

$$\check{K}_{6,5} = (Y_G - Y_{R,3})[-Z_G - \mu'_{3,x}(X_G - X_{R,3})] + (Y_G - Y_{R,2})[-Z_G - \mu'_{2,x}(X_G - X_{R,2})] + (Y_G - Y_{R,1})[-Z_G - \mu'_{1,x}(X_G - X_{R,1})] - \mu'_{3,y}(X_G - X_{R,3})(X_{R,3} - X_G) - \mu'_{2,y}(X_G - X_{R,2})(X_{R,2} - X_G) - \mu'_{1,y}(X_G - X_{R,1})(X_{R,1} - X_G)$$

$$\check{K}_{6,6} = (Y_G - Y_{R,3})^2 + (Y_G - Y_{R,2})^2 + (Y_G - Y_{R,1})^2 + (X_{R,3} - X_G)^2 + (X_{R,2} - X_G)^2 + (X_{R,1} - X_G)^2$$

where $(X_{R,i}, Y_{R,i})$ are the (X, Y) coordinates of point R_i and (X_G, Y_G, Z_G) are the coordinates of point G.